This is a repository copy of *Influencing the draping behaviour of solid epoxy prepregs by applying 3D-printed resin patterns*.

White Rose Research Online URL for this paper:
https://eprints.whiterose.ac.uk/id/eprint/231670/

Version: Published Version

---

**Article:**
Janzen, J., Schäfer, H., Celik, M. et al. (4 more authors) (2025) Influencing the draping behaviour of solid epoxy prepregs by applying 3D-printed resin patterns. Materials and Design, 259. 114780. ISSN: 0264-1275

https://doi.org/10.1016/j.matdes.2025.114780

---

**Reuse**
This article is distributed under the terms of the Creative Commons Attribution (CC BY) licence. This licence allows you to distribute, remix, tweak, and build upon the work, even commercially, as long as you credit the authors for the original work. More information and the full terms of the licence here: https://creativecommons.org/licenses/

**Takedown**
If you consider content in White Rose Research Online to be in breach of UK law, please notify us by emailing eprints@whiterose.ac.uk including the URL of the record and the reason for the withdrawal request.

eprints@whiterose.ac.uk
https://eprints.whiterose.ac.uk/

Materials & Design 259 (2025) 114780

Contents lists available at ScienceDirect

Materials & Design

journal homepage: www.elsevier.com/locate/matdes

# Influencing the draping behaviour of solid epoxy prepregs by applying 3D-printed resin patterns

Jan Philipp Janzen [a,*], Hendrik Schäfer [a], Murat Çelik [b], Colin Robert [c], Conchúr M. Ó Brádaigh [c], David May [d,a,1], Thomas Neumeyer [a]

[a] Leibniz-Institut fuer Verbundwerkstoffe GmbH, Erwin-Schroedinger-Str. 58, 67663 Kaiserslautern, Germany
[b] Faculty of Engineering, Mechanical Engineering Department, Erciyes University, 38039 Kayseri, Turkey
[c] Department of Materials Science and Engineering, University of Sheffield S10 2TN Sheffield, UK
[d] Faserinstitut Bremen e.V. (FIBRE), University of Bremen, Am Biologischen Garten 2 – Geb. IW3, 28359 Bremen, Germany

ARTICLE INFO

*Keywords:*
Prepreg
Epoxy
Woven
Draping
3D-printing
Bending
Picture-frame-test

ABSTRACT

This study presents a novel strategy to overcome the limitations of solid resin prepregs (SRPs) – namely the inability to drape at room temperature and hindered gas evacuation during vacuum-bag-only (VBO) processing – by 3D-printing a regular, uncured solid epoxy resin (SR) pattern on a dry woven textile. The locally patterned resin distribution preserves dry textile regions, enabling room temperature drapeability and more robust VBO-processing due to improved gas evacuation. By adjusting pattern parameters such as element geometry and coverage, the draping behaviour can be controlled to adapt to a desired draping condition. In order to be able to design the right pattern for given draping conditions, the influence of these parameters on bending and shearing was studied. Manual draping showed that bending radii down to 4 mm were achievable, governed only by the element length in bending direction, while coverage had no significant effect. In contrast, picture-frame-tests showed that the shearing is mainly influenced by the coverage and that a maximal shearing angle of 30° can be achieved. These results show that the SRPs bending and shearing can be independently influenced through pattern design. The derived structure–drapeability relationships enable targeted design of SRPs for robust, autoclave-free composite manufacturing.

## 1. Introduction

Fibre-reinforced polymer composites (FRPC) are key materials in lightweight structural applications, for example in aerospace, transportation, and renewable energy sectors. An established route to manufacture large FRPC structures involves the use of liquid thermoset prepregs, which require frozen storage, in a vacuum bag only (VBO) process. In this process, prepregs are laid up in a mould, sealed under a vacuum bag with auxiliary materials, and consolidated by applying vacuum pressure during oven or tool heating to initiate curing of the resin. However, due to the limited compaction pressure and the risk of prepreg ageing during layup, the VBO process is prone to pore formation. These pores reduce mechanical performance and typically result either from entrapped gases that couldn't get evacuated, or from increased resin viscosity caused by prepreg ageing [1–6]. Fig. 1 shows the flowchart of a typical VBO-process as well as the the cross section of a laminate with pores which resulted from entrapped gases.

A strategy to enhance the gas evacuation of the prepregs and mitigate pore development is to use semi-impregnated textiles, so called semipregs. For most semipregs the surface of the textile is fully impregnated but through the thickness it is only partially impregnated. Examples include Hexcel Corporation's "HexPly SuperFIT" [7–9], Solvay's "Carboform" [10] or Gurrit's "SPRINT" [11,12]. To further increase gas evacuation, new semipregs feature partially impregnated surfaces. This creates additional gas evacuation paths in the through-thickness direction of the prepregs, resulting in a higher gas permeability [13,14] which has been shown to reduce porosity in VBO processing [14–18]. Commercially available semipregs of this type are e.g. ZPreg from Solvay [10,19,20] or NTC-425 from NEXX-Technologies [21,22].

While these semipregs can help mitigate pore growth, they still require storage at frozen temperatures and remain sensitive to ageing effects. A possible solution for this is the use of solid resins (SR) instead

* Corresponding author at: Leibniz-Institut für Verbundwerkstoffe GmbH, Erwin-Schroedinger-Str. 58, 67663 Kaiserslautern, Germany.
*E-mail address:* jan.janzen@ivw.uni-kl.de (J.P. Janzen).
[1] Former affiliation.

https://doi.org/10.1016/j.matdes.2025.114780
Received 1 August 2025; Received in revised form 5 September 2025; Accepted 15 September 2025
Available online 16 September 2025
0264-1275/© 2025 The Author(s). Published by Elsevier Ltd. This is an open access article under the CC BY license (http://creativecommons.org/licenses/by/4.0/).

of liquid resins. In the field of FRPC SRs are used for fibre-reinforced 3D-printing [23,24], as a binder material for preform production, e.g. in dry fibre placement [25–27], as a moulding compound for integrative combination with prepregs in the injection moulding process [28–31] and especially as a matrix material for solid resin prepregs (SRP) and towpregs [15,32–44]. The advantage of SRPs is the combination of thermoplastic and thermoset processing properties: SRPs have a shelf life of more than two years at room temperature and can be liquefied and solidified multiple times, during which no relevant ageing occurs [15,39,41,45,46]. However, at elevated temperatures the SR reaches a low viscosity, allowing impregnation of the textiles at low-pressure levels. In addition, the exothermic heat generation during curing is lower than for liquid resins, which reduces the risk of thermal runaway in large structures. One drawback of SRPs is that they cannot be draped at room temperature due to the solid and brittle state of the uncured matrix. Currently, heating the complete SRPs is needed for draping which makes it difficult to mould large FRPC structures.

However, by applying a partial impregnation of the textile surface, comparable to the semipregs introduced, draping at room temperature can be achieved with the dry textile areas in the same way as in sliced sandwich cores or wood (see Fig. 2, right). In previous studies we showed that using these SRPs can mitigate the challenges with prepreg ageing, pore growth in VBO processes, and that a general drapeability at room temperature can be achieved [15,47]. By adapting these patterns, the drapeability may not only be improved globally, but could also be adjusted locally according to a given draping condition. In order to fully utilize the potential and to be able to design the right pattern for the given draping condition, a general understanding of how the pattern affects draping is required.

### 1.1. Objective of this work

The aim of this work is to investigate whether the patterns on the SRPs can be designed in such a way that it is possible to mould single curved parts via bending or multiple curved parts via bending and shearing at room temperature. For this the influence of different patterns on the draping behaviour of SRPs has to be investigated so that general pattern design guidelines for given draping conditions can be developed. These findings may also support the local control of drapeability in dry textiles or preforms via local binder application, helping to minimise defect formation. In addition, this study examines whether the approach described by Turk et al. in [48] – redirecting shear to target regions without compromising bending by applying localised resin patches to dry fabrics – can also be achieved through targeted pattern design. To achieve this, different SR patterns were 3D-printed onto two woven fabrics and their draping behaviour was investigated.

### 1.2. State-of-the-art

#### 1.2.1. 3D-Printing solid epoxy resins

Epoxy based SRs are fully reactive resin systems (including resin and hardener) that are solid, brittle, and tack-free at room temperature and are usually available in the form of powders or granulates. The SRs can be liquefied and resolidified multiple times without the occurrence of any significant crosslinking reaction, which is why they can also be used in the field of 3D printing [39,41,45,46]. Epoxy-based SRs are mainly used in industry in the fields of powder coating and component manufacture without fibre reinforcement by means of injection moulding, pressing or transfer pressing [49,50]. In addition to processing on an industrial scale, SRs are used in the research field of additive manufacturing and in niche areas of fibre-reinforced plastic composites. Drücker et al. produced filaments from SR and processed them in a FDM printer [51]. However, the brittleness of SR posed a problem, resulting in filament breakage during the feeding step. For this reason, the SR filament had to be fed through a tube to the extruder unit using a thermoplastic filament. Due to the high cost of filament production and the limited printing volume, the process is not used outside research. An alternative approach was pursued by Shen et al. who extruded the SR with heated syringe pumps, also known as direct-ink writing [52]. Wimmer et al. also used direct-ink writing, but with so-called “semi-solid resins”, a blend of SR and liquid epoxy resins [53]. Direct-ink writing can increase the print volume compared to the method described in [51], but is still limited by the syringe pump volume. Jiang et al. also used a syringe pump extruder to process SR with carbon nanotubes, and they also used a single-screw extruder to print SRs [54]. The main advantage of the single screw extruder is the ability to continuously feed SR and thus overcome the problem of limited print volumes.

#### 1.2.2. Draping

In order to mould 3D-structures with 2D-semi-finished products such as prepregs, they must be able to deform. This process is also known as

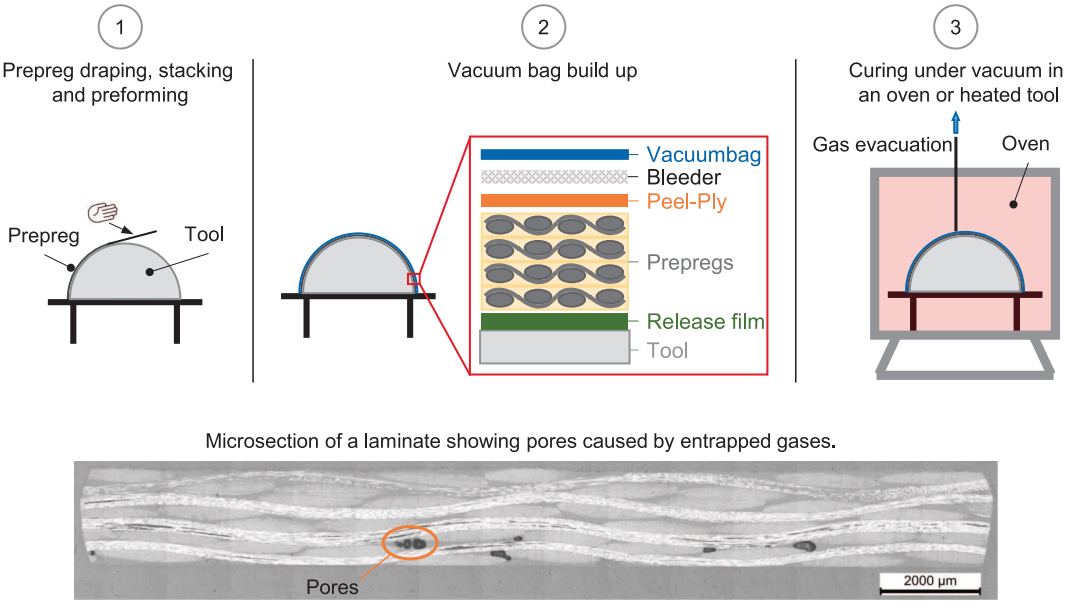


**Fig. 1.** Flowchart of a VBO-process (top); Microsection of a VBO-laminate with typical defects (bottom).

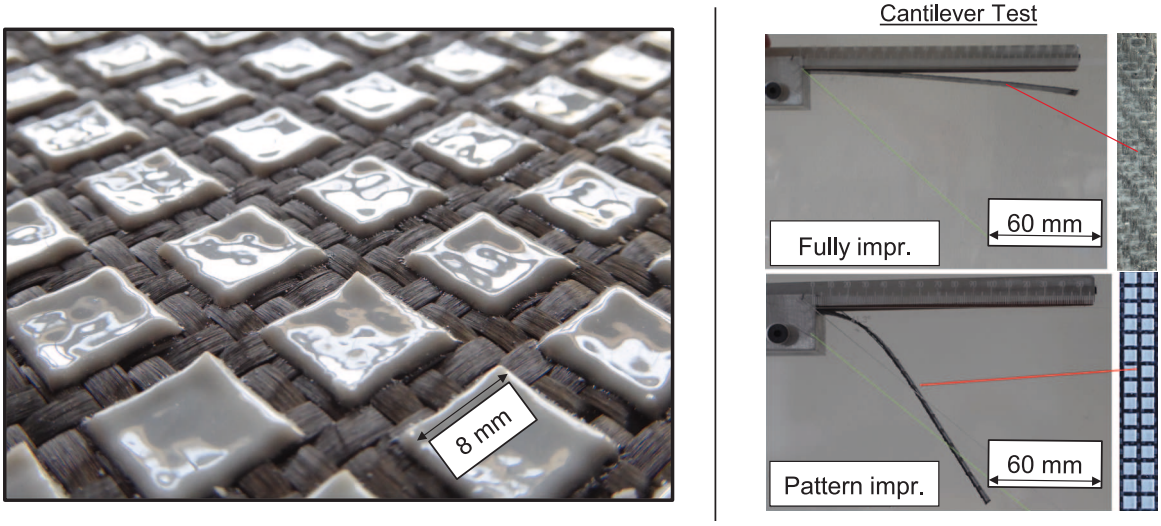


**Fig. 2.** Left: SRP with quadratic pattern and a coverage of 60%; right: comparison of draping a fully impregnated SRP and a SRP with pattern impregnation.

draping, during which the prepregs usually undergo deformation in the form of bending and shearing. Draping is a quality-critical process, since process errors can lead to imperfections such as fibre undulations, wrinkles or misaligned fibres. These imperfections can have a significant influence on the mechanical properties [55–57]. In order to minimise these process errors, the underlying draping properties of the prepregs must be known. Cantilever test is widely used [55,58–61] in order to determine the bending stress and stiffness of the prepregs, which among other properties are relevant for draping simulations. With the help of a slider, the specimen is pushed evenly over the support surface within ten seconds until it protrudes beyond it and reaches the predefined angle of 41°30′ (see Fig. 3). The slider position can then be used to determine the overhang length and calculate the bending stiffness. This allows the bending behaviour to be quantified and enables simulative prediction. Further developments of the cantilever test often use a freely suspended specimen without reaching a predefined angle and approximate the bending using higher order polynomials or splines [55,62]. In the cantilever test, a linear relationship is assumed between the bending moment and the curvature of the textile.

In addition to the bending behaviour, the shearing behaviour of the prepregs is of crucial importance during draping. Particularly when moulding double-curved geometries, the prepregs must undergo a shearing process in which the fibre orientation and the angle between fibres change. An established test method for investigating shear behaviour is the picture-frame-test [59,60,63–67]. For the picture-frame-test, a square test specimen with corner cut-outs is clamped in a picture-frame rig (Fig. 4). The picture-frame rig is integrated into a universal testing machine and enables the application of pure shear stress in the plane of the specimen. The recorded force–displacement curve can then be used to determine the force-shear angle curve. In addition to the force required to generate a certain shearing and the resulting fibre orientation, the so-called “locking angle“ is an evaluation criterion for shearing behaviour. The locking angle describes the angle

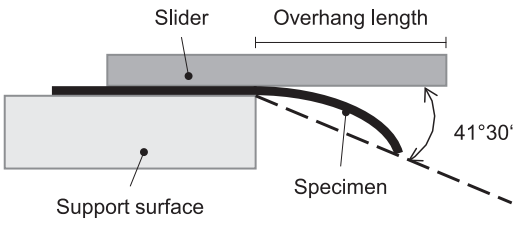


**Fig. 3.** Cantilever test setup.

at which the rovings of the textile are pushed together to such an extent that the textile bulges and wrinkles occur. It is defined as the apex of the force-shear angle curve and is determined by two intersecting tangents that originate from the linear parts of the curve (Fig. 4). Shearing the textile beyond the locking angle is not recommended due to the reduction in mechanical properties associated with the formation of wrinkles. The fibre orientations and angles are usually calculated by using the machine path or imaging methods.

The resulting fibre orientation after draping is of particular interest when moulding complex, multi-curved structures due to its significant influence on the mechanical properties of fibre-reinforced-plastic (FRP) components. When moulding complex, multi-curved structures, the risk of defects in the form of deviating fibre angles, undulations and wrinkles is the highest. Efforts are therefore being made to locally influence the draping behaviour of textiles or prepregs and thereby redirect the shearing from critical component areas to non-critical ones. Influencing the drape properties is mainly achieved by introducing sewing, tufting or binder patterns [48,68–73]. Shen et al. were able to significantly reduce the formation of wrinkles during the moulding of square-box and hemispherical tools by tufting textile semi-finished products or shifting them to mechanically uncritical edge areas [69].

Turk et al. attempted to prevent defects in draping by applying a liquid epoxy binder pattern at different curing levels [48]. By applying the binder pattern, they showed that it is possible to redirect the fabric shear to non-critical component areas and to reduce wrinkling and fibre disorientation. The binder patterns were applied specifically in areas where a high shear angle was expected. The binder pattern led to a stiffening of these fabric areas, resulting in a shift of the shearing to dry textile areas. However, the influence of the binder pattern on the bending properties of the fabric posed a challenge. If the bending stiffness is increased too much, it is no longer possible to mould tight radii. Therefore, they concluded that the binder patterns should ideally prevent shearing but have as little influence as possible on the bending properties. In addition, it was suggested that the local influence of the binder patterns on the draping behaviour must be known in order to fully exploit their potential.

Turk et al. therefore investigated the shear behaviour of fabrics with binder patterns using bias-extension tests and used the results as parameter input for draping simulations [74]. However, the results and the scope of the tests proved to be too inaccurate to be able to carry out meaningful simulations. It was also not possible to predict the fibre orientations in dependence of the pattern. Therefore, there is still a need for further research in this area and also with regard to the resulting bending properties of the semi-finished products.

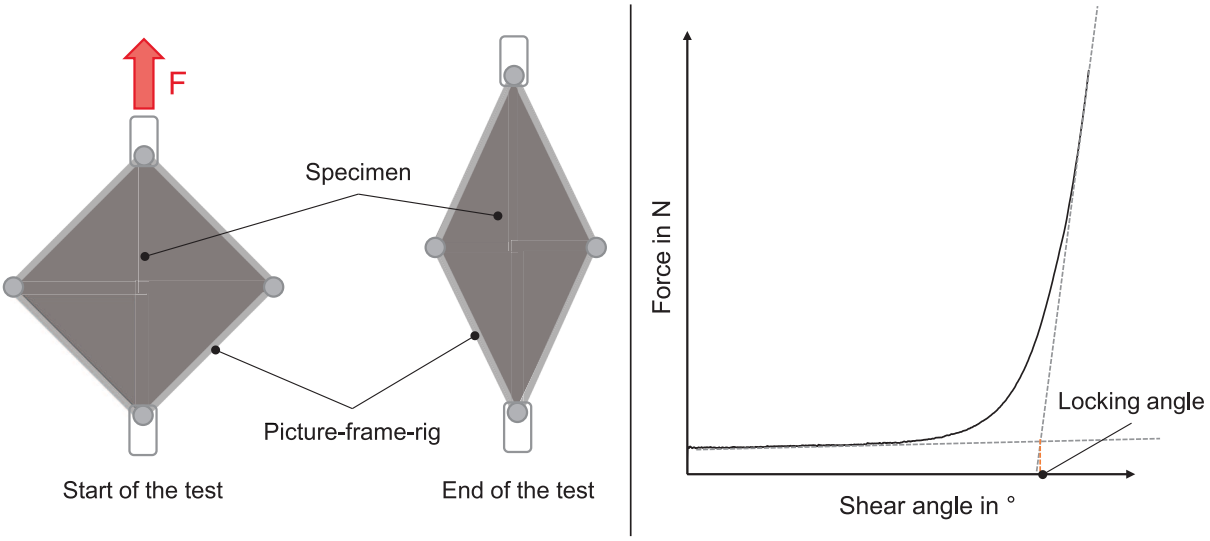


**Fig. 4.** Left: picture-frame-test setup; right: determination of the locking angle.

## 2. Materials & methods

In the following section, the materials and methods used are explained as well as the manufacturing of the SRPs. In order to characterise the bending behaviour of the SRPs, a new test method was developed, since the cantilever-tests were found to be unsuitable due to the inhomogeneous areal weight distribution of the SRPs. The shearing behaviour was characterised by conducting picture-frame-tests. During these tests the fibre orientation was determined by using a polarisation camera.

### 2.1. Materials

The epoxy based SR-system E1040 by Swiss CMT AG are used for all tests. The SR comes in a granulate form and has a density of 1.2 g/cm$^3$. Fig. 5 shows an exemplary DSC curve of the system for a heating rate of 10 K/min in a nitrogen atmosphere. It can be seen that the uncured SR has a glass transition temperature ($T_g$) of 42 °C and that the curing reaction starts at approximately 150 °C. After curing the SR for 30 min at 180 °C, it has a $T_g$ of 108 °C, a tensile strength of 78 MPa and a Young modulus of 3.2 GPa.

Two balanced woven fabrics were used in this study, the twill 2/2 glass fibre (GF) fabric HexForce 01,102 100 TF970 from Hexcel and the twill 2/2 carbon fibre (CF) G-Weave from Lange and Ritter. Table 1 compares the two fabrics.

### 2.2. SRP manufacturing

The SRPs were manufactured using a modified Ender 5 Pro 3D-printer from Creality. The existing filament extruder was replaced by a

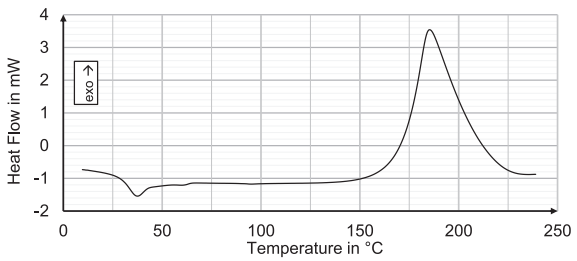


**Fig. 5.** DSC curve for the E1040 at a heating rate of 10 K/min in nitrogen atmosphere.

**Table 1**
Comparison of the woven fabrics.

| Fabric | Areal weight | Thread count | Titer |
|---|---|---|---|
| GF – Hexcel 01,102 | 290 g/m$^2$ | 7 cm$^{-1}$ | 1 K roving with 68 tex |
| CF – G-Weave | 200 g/m$^2$ | 5 cm$^{-1}$ | 3 K roving with 198 tex |

newly developed extruder unit with an extruder screw (see Fig. 6). A stainless steel extruder screw with a diameter of 8 mm and a length of 82 mm is used to convey the granulate. It is connected to a NEMA17 stepper motor with a 5:1 planetary gearbox via a shaft coupling. Due to the short shaft length, the decision was made to implement a so-called "hot barrel" design, in which the entire material is melted in the aluminium material storage [75]. This prevents clogging of the conveying area due to agglomerated granulate, which can occur if the temperature gradient between the heating zone and the material storage is not high enough. The melting of the granulate is achieved by using a heating cartridge which has been inserted to the heat block.

The printer's maximum printing area is 200 x 200 mm2. The extruder unit was moved relative to the textile for printing. Table 2 lists the printing parameters used for the SRP manufacturing.

The printing accuracy was determined by measuring the edge lengths of the pattern elements with the 3D-scanning tool of a Zeiss Smartzoom 5 digital microscope. The deviations of the edge lengths were ± 0.3 mm from the target length. After printing the SR sits on top of the textiles like a coating with almost no micro impregnation into the rovings. The patterns all had quadratic pattern elements with different edge lengths and degrees of coverage (fraction of the textile surface covered by the pattern). The used coverages of the textiles were 20, 40, 60 and 80 %, the edge lengths of the squares were 4, 6, 8 and 10 mm, all with a height of 0.64 mm, resulting in different fibre volume contents (FVC) for the specimens. The patterns investigated in this study with different coverages and pattern element edge lengths are shown in Fig. 7.

### 2.3. Characterisation methods

#### 2.3.1. Formable radii

The developed method to characterise the bending behaviour identifies the minimal formable radii. The aim of the tests is to find out how the pattern properties influence the radii that can be draped at room temperature in a manual lay-up and to determine guidelines for the

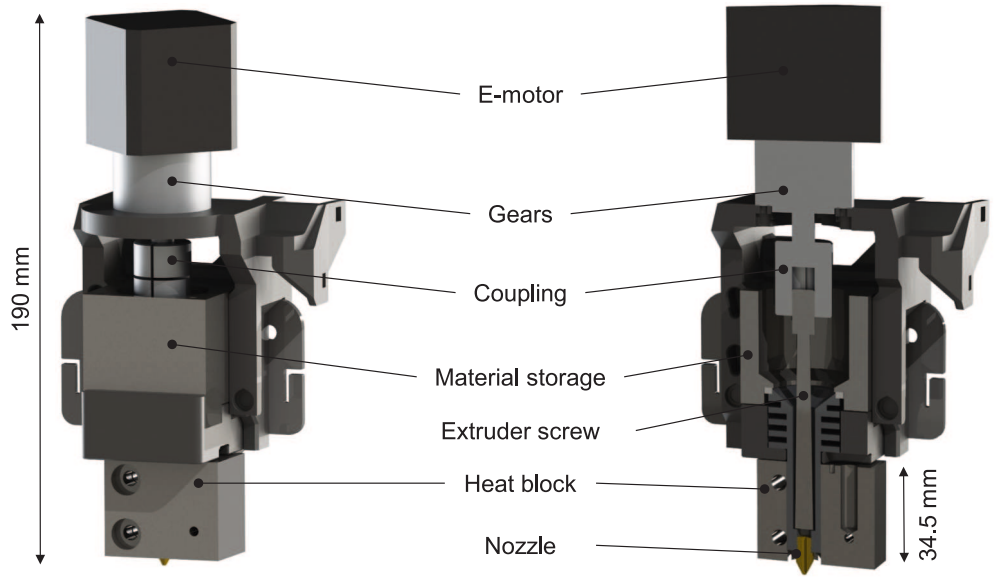


**Fig. 6.** Developed extruder unit with extruder screw (left) and its sectional view (right).

**Table 2**
Printing parameters for the SRP manufacturing.

| Parameter | Value |
|---|---|
| Nozzle diameter | 0,50 mm |
| Layer height | 0,32 mm |
| Printing speed | 30 mm/s |
| Nozzle temperature | 105 °C |
| Print bed temperature | 50 °C |

pattern design based on the results. To evaluate these radii, the SRPs were manually draped around 3D-printed tools (Fig. 8). Four different tools were printed with radii of 10, 14, 18 and 22 mm. The SRPs were draped over these radii with the pattern facing upwards as well as downwards, in order to reproduce both the draping of concave and convex radii. The SRPs were pulled over the tools by hand, no additional forces were used to make the SRPs fit the tool.

Fig. 9 shows draping tests that are deemed valid and invalid. A test is valid when the SRP can be draped over the 3D-printed tool without the occurrence of a polygon effect (see invalid (a)) or a detaching of pattern elements from the textile (see invalid (b)). The test specimens were 110 mm long and 20 mm wide. A row of complete pattern elements was printed in the centre of each specimen; the adjacent pattern elements were only partially printed if they did not fit completely into the 20 mm wide cut-out. The textile used was the GF fabric from Hexcel. For each coverage and edge length configuration three specimen were tested.

### 2.3.2. *Picture-frame-test*

The picture-frame-tests were carried out according to DIN EN ISO 20337:2020-01 [64]. The general test procedure is explained in the state

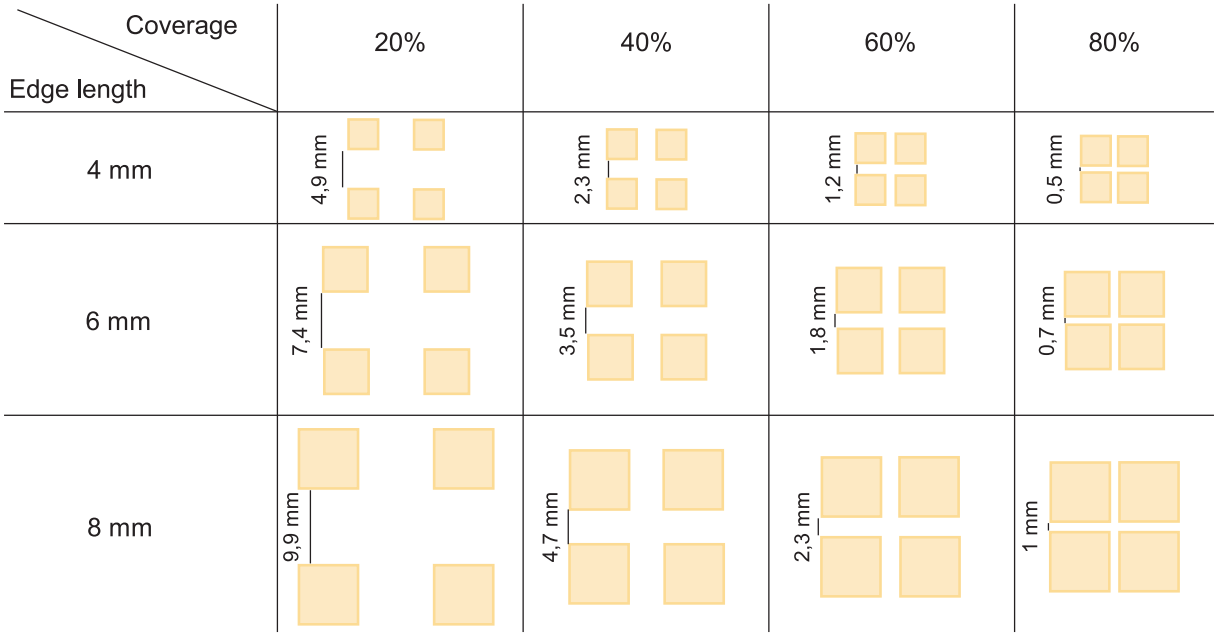


**Fig. 7.** Depiction of resin patterns with varying coverages and pattern element edge lengths. Patterns with a 10 mm edge length are omitted due to size constraints.

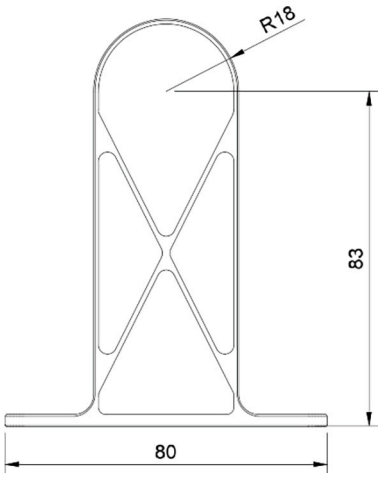


**Fig. 8.** 3D-printed tool with a radius of 18 mm (all values are in mm).

of the art, the used sample geometry is shown in Fig. 10. The holes for clamping the samples in the shear frame have a diameter of 10 mm. The patterns were printed onto the center of the specimen (size of the printed area: 100 × 100 mm$^2$). The clamping areas of the SRPs were stabilised with a thermoplastic binder (Spunfab PA1541 with 12 g/m$^2$) to prevent fraying. In order to achieve uniform clamping, sealing cords with a diameter of two millimeters were inserted into the clamping areas. The Hexcel GF fabric was used for the tests, as reference the dry textile was tested as well. The force-shear-angle curves were determined using a picture-frame rig which is mounted to a universal testing machine by Zwick with a load cell of 2.5 kN. The test speed was 50 mm/min. For each coverage and edge length configuration three specimen were tested.

#### 2.3.3. Picture-frame-test with polarization camera

The aim of using a polarisation camera to analyse the picture-frame-tests is to quantitatively identify the fibre orientation of CF-SRPs during shearing. The polarisation camera used was the C5S-MP developed by Alkeria, which can measure and visualise the fibre orientation of CF. The camera utilises the CF's polarisation effect, whereby natural, unpolarised light that hits the CF is reflected as polarised light. The polarisation angle of the reflected light is thus correlated to the CF orientation. The camera measures the degree of linear polarisation (DOLP) to determine the region of interest as well as the angle of linear polarisation (AOLP) which corresponds to the angle of orientation of the CF. [76,77].

To analyse the fibre orientation for different shearing angles, the polarisation camera was placed orthogonally to the dry backside of the specimen in order to record the DOLP and AOLP images. These images were each taken for every 10 mm of machine displacement. Table 3 shows the corresponding shearing angles.

False colour images were then derived from the AOLP images as well as a fibre orientation histogram (see Fig. 11). In contrast to the previous tests, all samples had an edge length of 8 mm. In order to be able to use the polarization camera, the CF textile had to be used for the tests instead of the GF textile.

## 3. Results & discussion

### 3.1. Formable radii

Table 4 shows the results of the draping tests. The table is divided horizontally according to the type of draped radius, inner or outer radius, and vertically according to the size of the radius. The results are displayed in the form of a matrix in which the coverage is displayed on the horizontal and the edge length of the pattern elements on the vertical. Combinations for which the test results were assessed as valid are labelled as "1″ and highlighted in green. Combinations for which the test results were assessed as invalid are either labelled as "a" or "b" according to the respective exclusion criterion and highlighted in orange.

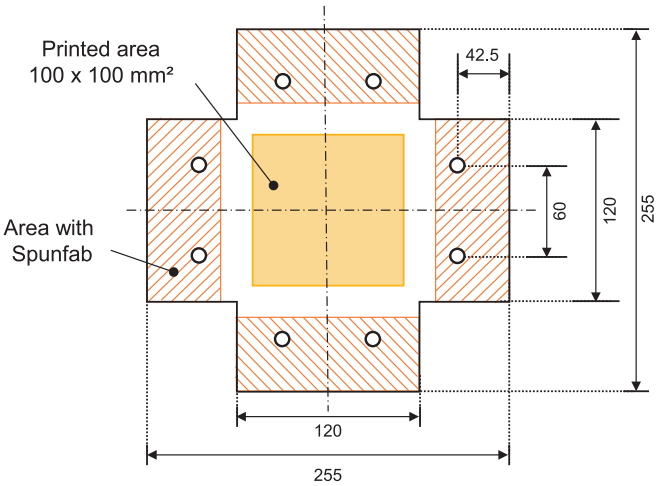


**Fig. 10.** Geometry of a shearing specimen (all values are in mm).

**Table 3**
Machine displacement and corresponding shearing angles.

| Machine displacement in mm | 0 | 10 | 20 | 30 | 40 | 50 | 60 | 70 |
|---|---|---|---|---|---|---|---|---|
| Shearing angle in ° | 0 | 5.2 | 10.6 | 16.4 | 22.6 | 29.4 | 36.9 | 45.6 |

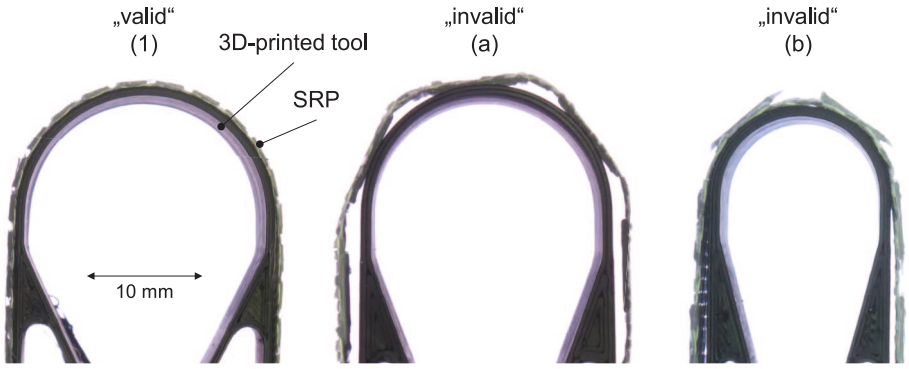


**Fig. 9.** Schematic depiction of valid and invalid draping tests.

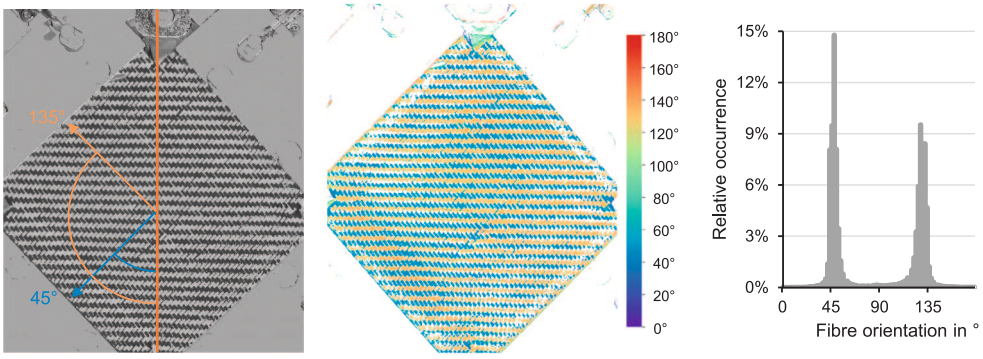


**Fig. 11.** AOLP image taken by the polarisation camera at the starting position and definition of the fibre orientations (left), false colour image created (centre), resulting fibre orientation histogram (right).

**Table 4**
Result matrix of the draping tests, (1) valid test, (a) invalid due to polygon effect, (b) invalid due to detachment of the pattern elements.

| Radius | Coverage Edge length | Concave radius 20 % | 40 % | 60 % | 80 % | Convex radius 20 % | 40 % | 60 % | 80 % |
|---|---|---|---|---|---|---|---|---|---|
| 22 mm | 4 mm | 1 | 1 | 1 | 1 | 1 | 1 | 1 | 1 |
| | 6 mm | 1 | 1 | 1 | 1 | 1 | 1 | 1 | 1 |
| | 8 mm | 1 | 1 | 1 | 1 | 1 | 1 | 1 | 1 |
| | 10 mm | 1 | 1 | 1 | 1 | 1 | 1 | 1 | 1 |
| 18 mm | 4 mm | 1 | 1 | 1 | 1 | 1 | 1 | 1 | 1 |
| | 6 mm | 1 | 1 | 1 | 1 | 1 | 1 | 1 | 1 |
| | 8 mm | 1 | 1 | 1 | 1 | 1 | 1 | 1 | 1 |
| | 10 mm | a | a | a | a | a | a | a | a |
| 14 mm | 4 mm | 1 | 1 | 1 | 1 | 1 | 1 | 1 | 1 |
| | 6 mm | 1 | 1 | 1 | 1 | 1 | 1 | 1 | 1 |
| | 8 mm | a | a | a | a | b | b | b | a |
| | 10 mm | a | a | a | a | b | b | a | a |
| 10 mm | 4 mm | 1 | 1 | 1 | 1 | 1 | 1 | 1 | 1 |
| | 6 mm | a | a | a | a | b | b | b | b |
| | 8 mm | a | a | a | a | b | b | b | b |
| | 10 mm | a | a | a | a | b | b | a | a |

As can be seen, the coverage of the pattern has no influence on the achievable radii. As soon as the edge length of the pattern elements is too large, the radius can no longer be formed regardless of the coverage used. The bending behaviour is therefore mainly influenced by the edge length of the pattern element in bending direction. An exception to this would be an edge length-coverage radius combination in which the distances between the individual pattern elements are so large that the radius can be formed completely from the dry textile areas between the elements.

The independence of the results from the coverage can be explained by using an analogy to chain drives. The behaviour of the SRPs which are draped over the tools is similar to a chain that is wrapped around a gear. The pattern elements behave like the rigid chain links, whereas the dry regions behave like the bearing pins (see Fig. 12).

In this analogy the coverage of the SRPs would be close to 100 % as there are only minimal distances between the chain links. The radius to be formed is equivalent to the gear around which the chain is wrapped. Due to the rigid areas of the chain or SRP, a polygon is always produced when forming a radius. The center of these rigid areas usually depicts the radius to be formed $r$, whereas the dry areas or bearing pins form a larger radius $r_{max,}$ which represents the largest deviation from $r$ as well as a corner of the polygon (see Fig. 12). The greater the difference between $r$ and $r_{max}$, the more pronounced the resulting polygon effect and the worse the target radius formed. In the case of chain drives, this leads to uneven running; in the case of SRPs, this results in high fibre undulations and wrinkling in the manufactured component. The polygon effect is

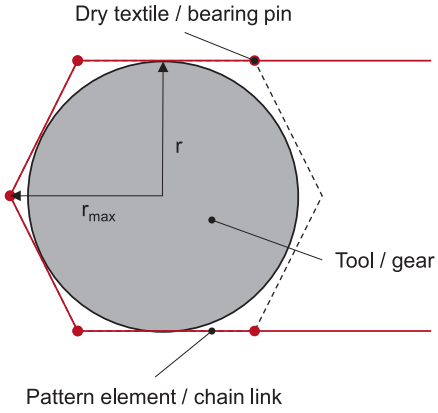


**Fig. 12.** Illustration of the analogy between SRPs and chain drives.

quantified for chain drives using the so-called degree of non-uniformity [78,79]. In analogy to the degree of non-uniformity, a relative error $e$ is defined for the SRPs as the difference between $r$ and $r_{max}$ in relation to $r$:

$$e = \frac{r_{max} - r}{r} \tag{1}$$

where $r_{max}$ can be calculated using the number of pattern elements $n_M$ with equation (2) which results from the trigonometric relationships between $r$ and $r_{max}$:

$$r_{max} = \frac{r}{\cos\left(\frac{\pi}{n_M}\right)} \tag{2}$$

By inserting equation (2) into equation (1), it can be seen that $e$ is independent of the radius $r$ and is only influenced by the number of pattern elements used to form the radius. Equation (3) was used to determine the minimal number of pattern elements ($n_{min}$) needed to form the minimal formable radius ($r_{min}$) for a given edge length ($L_{edge\ length}$). It was derived from the assumption that the circumference of the formed circle is approximately equal to the length of the pattern elements times the number of pattern elements:

$$r_{min} \approx \frac{L_{edgelength} * n_{min}}{2 * \pi} \tag{3}$$

To use this equation as a design guideline the minimal number of pattern elements $n_{min}$ must be known. To determine the minimal number of pattern elements $n_{min}$ to form a circle, equation (3) and the bending test results were plotted together in Fig. 13. Equation (3) is shown as two linear graphs – one for 11 and one for 12 pattern elements – while the experimental data is depicted as green circles for valid tests and as red crosses for invalid tests. The goal was to find the minimal number of

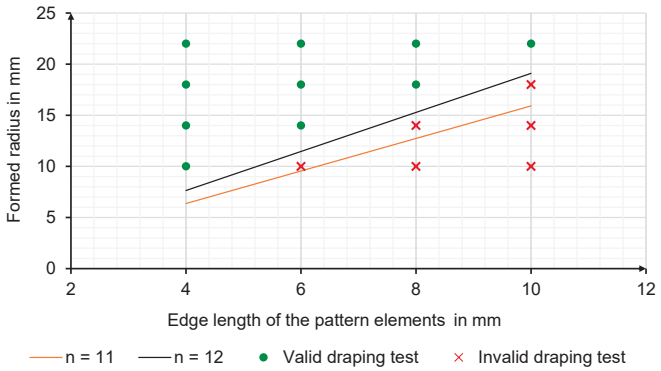


**Fig. 13.** Equation (3) with different pattern element numbers and results of the draping tests.

elements for which the linear graph separates the test results, so that the valid tests are above the graphs line and all invalid tests are underneath it. This was achieved with a minimal pattern element number of 12 resulting in a maximal acceptable relative error *e* of 3.53 %. As a result, equation (3) can now be used as a design guideline to determine the required pattern edge length for a given target radius.

### 3.2. Picture-frame-test

Fig. 14 shows four graphs in which the shear force is depicted over the shear angle for the GF-reinforced SRPs and the dry textile. Each of them shows the curves for the tested edge lengths with the same coverage as well as the curve for the dry textile. The standard deviations are shown as transparent areas. The dry textile has the lowest required forces and the lowest standard deviation. Furthermore, its locking angle is approximately 45°. For the SRPs the standard deviations of the curves intercept each other for all coverages, indicating that the edge length has no significant influence on the force-shear-angle curves. However, the coverage influences the detachment behaviour of the pattern elements as well as the curves, as the needed shear forces rise with an increase in coverage. With coverages of 20 and 40 %, there is no or only slight pattern detachment during shearing, whereas the pattern detaches over a large area in SRPs with coverages of 60 and 80 % at high shear angles. This can also be seen in the corresponding graphs in form of a decrease in shear force. While the forces are greater for the 20 and 40 % SRPs than for the dry textile, the curve progressions are similar.

There is initially a slight increase in force until the shear angle reaches the locking angle, where the shear forces increase rapidly. This is due to the fact that the pattern elements block the shearing of the textile locally and absorb the shear forces. For coverages of 60 and 80 % and a shear angle of approximately 30°, the shear force reaches a local plateau at which the pattern elements are pushed against each other and the stress inside them becomes so great that they break and detach from the textile. As a result, there is an initial drop in force and a shearing of the textile occurs in the areas where the patterns break. As the shear angle increases further, the force increases again as the locking angle is reached.

The force-shear-angle-curves can therefore be used to derive the maximum shear angle at which large-area detachment of the pattern occurs. Besides the force-shear angle curves, the resulting fiber orientations are an important aspect, which is discussed in the following section.

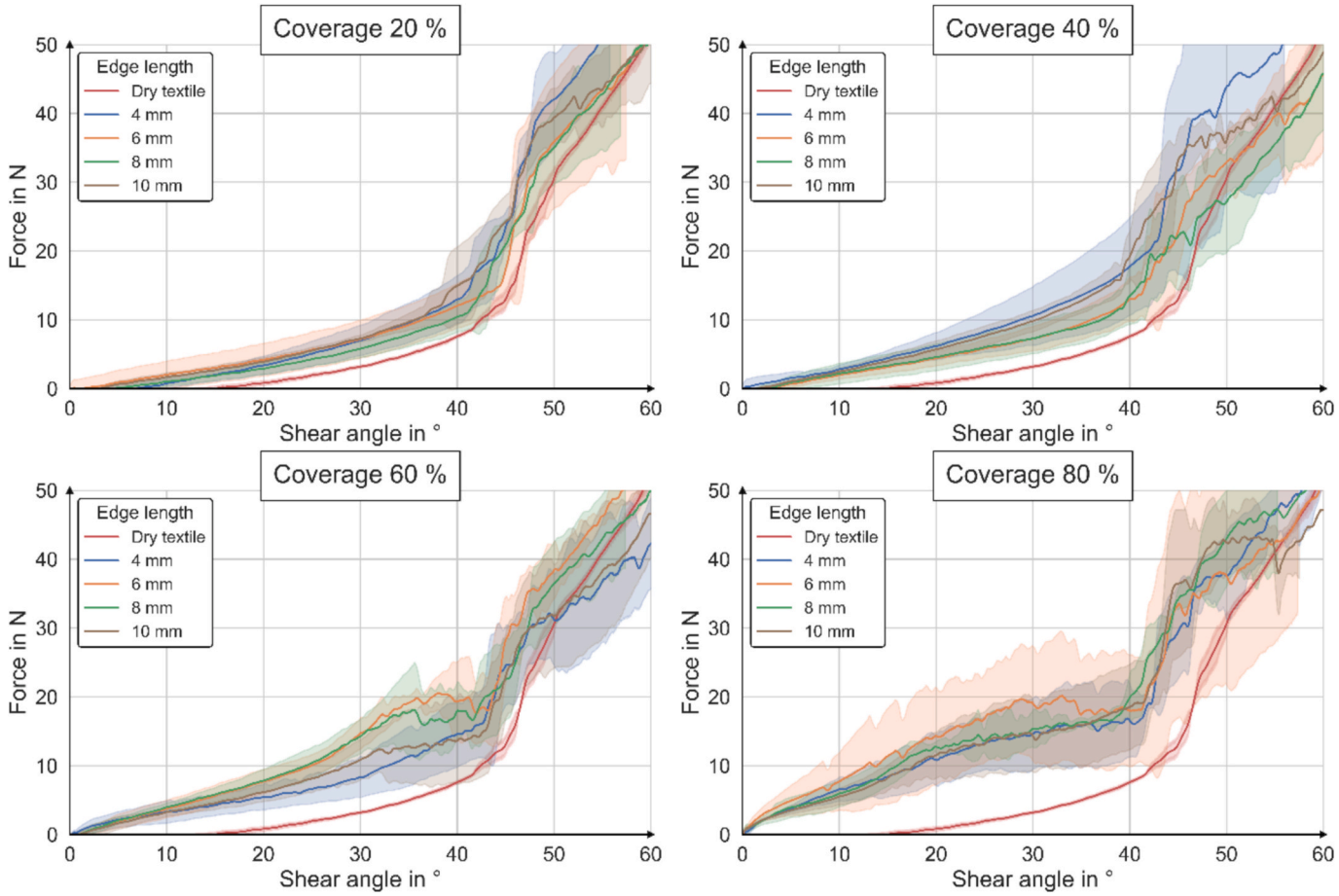


**Fig. 14.** Influence of coverage and edge length of the pattern element on the force-shear-angle curves.

### 3.3. Picture-frame-test with polarisation camera

The analysis of the fibre orientation with the polarisation camera showed that in the dry CF textile, a homogeneous fibre orientation with two main orientations across the shear surface can be seen during the shearing tests. At the beginning of the test, the main orientations of the fibres are approximately 45° and 135°, at the end approximately 25° and 155°. This can also be seen in the fibre orientation histograms, in which two distinct peaks move apart with increasing shear angle. For the SRPs, the pattern elements locally block the shearing of the textile. This can also be seen in the images of the polarisation camera. For coverages of 20 and 40 %, this leads to a local highly inhomogeneous fibre pathways, which are not desirable in terms of mechanical performance (see Fig. 15 for a 20 % SRPs). In the corresponding histograms, the peaks flatten and widen as a result of the inhomogeneity. This flattening is mainly due to the fact that the depicted peaks actually consist of two overlapping peaks. One of these peaks represents the dry areas, the other the areas blocked by the pattern elements.

In comparison, for high coverages of 60 and 80 % two homogenously sheared areas form, one in the printed area and one in the dry edge regions. These two areas form as the shearing is also blocked in between the pattern elements due to the small distances between them. The shearing of the SRP is therefore realised almost exclusively in the dry edge area, which is why there is a greater change in the fibre orientation (see Fig. 15 for an 80 % SRPs).

As soon as a shear angle of approximately 30° is reached, the pattern begins to break and to detach from the textile. In the areas where the pattern breaks and detaches from the textile, the fibres are no longer fixated and shear as a result. This can also be seen in the false colour images in Fig. 15. The detachment of the pattern is not caused by insufficient adhesion between the textile and the resin elements, but rather by the fact that, at high shear angles, the individual elements are increasingly pressed against each other and subsequently fracture as a result of the induced stresses. This fracture of the elements then leads to partial or complete detachment of these elements. The experiments with 20 % and 40 % coverage further demonstrate that the adhesion is sufficient, as no detachment of the pattern elements occurs in these cases. An increase in adhesion between the pattern and the textile would therefore have no effect on the detachment, since the limiting factor is the mechanical properties i.e. the resin cohesive strength of the uncured resin system. An increase in the cohesive strength could improve process stability and shift the pattern element detachment to higher shear angles. However, an increase in the shear angle can only be achieved until the locking angle is reached in the dry edge areas as a result of the shear relocation.

The shear relocation to the dry edge areas leads to a further flattening of the peaks in the histograms. To illustrate this for an 80 %-SRPs, the fibre orientation histograms of the printed area and the dry edge area are shown in Fig. 16. For reference, the histograms of a dry textile are depicted as well.

Compared to the peaks of the dry textile, both areas of the SRP already show lower and flatter peaks at a shear angle of 5.2°. As the shear angle increases, the shear redirection becomes more apparent in the fibre orientation histograms of the 80 %-SRP. While the printed area deviates only slightly from the starting orientations of 45° and 135° until the pattern breaks, the peaks of the edge area move further and earlier

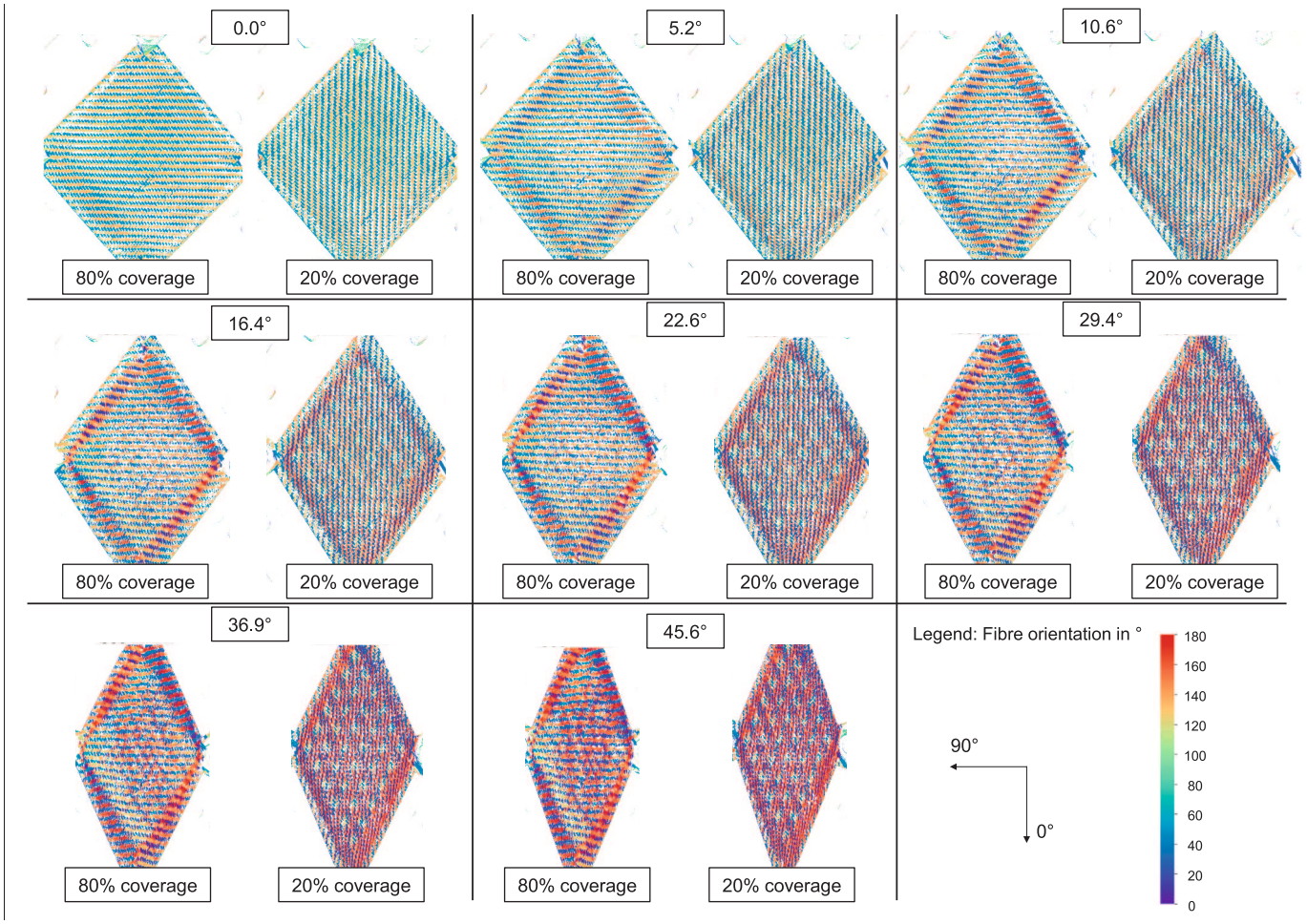


**Fig. 15.** Comparison of the fibre orientations of SRPs with 80% and 20% coverage for different shearing angles.

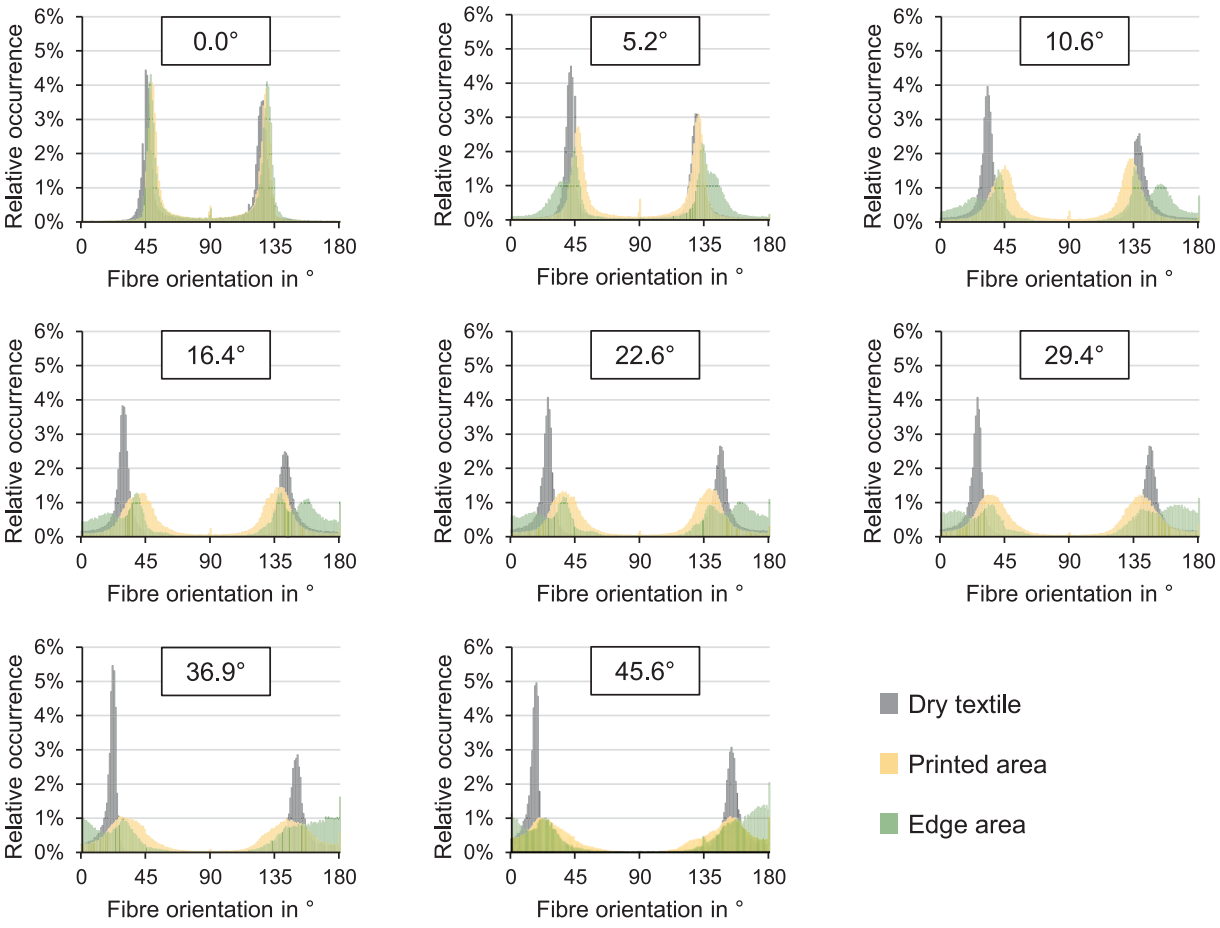


**Fig. 16.** Comparison of the fibre orientation histograms of the printed area, the dry edge area of a 80%-CF-SRP and the dry CF-textile.

apart than those of the dry textile. By applying a pattern with a high coverage or in other words small distances between the pattern elements, the shearing can be directed to dry SRP areas. In the production of FRP components, this can be used to direct the shearing to non-critical component regions, analogous to the methods presented in section 1.2.

However, it will still be challenging to produce double curved components where high levels of in-plane shear are required, especially when large regions of the fabric are not impregnated. The maximum size of the unprinted regions that can still be impregnated in a VBO process depends on various prepreg and process parameters. These include among others the permeability of the textile, the fibre mass content of the SRPs, the pattern design as well as the heating rates and holding times used. The analysis of these parameters and the moulding of double-curved parts are subject of subsequent studies.

## 4. Conclusions & outlook

In this study, the draping properties of SRPs at room temperature were evaluated by investigating the bending and shearing behaviour in dependence of the pattern design. Overall, it was shown that the partial impregnation in pattern form enables forming of the SRPs at room temperature and that the pattern design can be used to control the draping behaviour. The bending behaviour can be significantly influenced by adjusting the pattern edge length in the bending direction. The smaller the pattern edge length in the bending direction, the smaller the radii that can be formed. The coverage of the pattern plays a less pronounced role in bending. However, for small bending radii, a reduction in the coverage can be utilised in such a way that the dry areas between the pattern elements are large enough to form the complete radius. Using equation (3), the pattern edge length can be calculated for a radius to be formed, thus serving as a design guideline for the pattern. With this, it is possible to form components that involve multiple radii but require little to no in-plane shear—such as, for example, an Omega-profile.

In contrast, the shearing is primarily influenced by the coverage, while the pattern element size has no significant influence on the required shearing forces. For small shear angles of less than 10°, any pattern design can be used. For larger shear angles, the pattern should be designed in such a way that a coverage of at least 80 % is used in areas where no shearing should occur. This allows the shearing to be directed into non-critical component regions. In order to enable shearing in these regions and to achieve a homogeneous fibre orientation, no pattern should be printed onto these regions. The maximum size of the unprinted regions that can still be impregnated in a VBO process depends on various prepreg and process parameters. These include among others the permeability of the textile, the fibre mass content of the SRPs, the pattern design as well as the heating rates and holding times used. The analysis of these parameters and the moulding of double-curved parts are subject of subsequent studies.

The conclusions drawn in this study are not limited to the fibre materials investigated. Applying a solid resin pattern inevitably reduces the drapeability compared to the dry textile, which therefore represents the upper limit of formability. For instance, if the dry textile can only be formed to a minimum bending radius of 5 mm, no patterned SRP will enable forming to a smaller radius. However, for geometries with radii above this material-specific limit, the structure–drapeability relationships identified here remain valid and can be applied irrespective of the underlying fibre material.

The findings of this study are not only useful for the design of prepregs with a pattern impregnation, but also for influencing the

drapeability of dry textiles or preforms through the application of binder materials. As stated in the state of the art, the general aim of influencing the draping of these materials is to shift the shearing to non-critical component areas without influencing the bending properties [48,74]. This study was able to show that this is possible, as the shearing is mainly influenced by the coverage, while the bending properties are only influenced by the pattern edge length. Therefore, the shearing can be influenced by adjusting the coverage while simultaneously enabling bending by applying pattern elements small enough to form a given radius.

In practical terms, the findings of this study provide explicit guidelines for the design of SRPs to achieve targeted draping behaviour in components. Designers can control bending by selecting pattern elements with an appropriate edge length in the bending direction, as calculated using equation (3), to achieve the desired minimum radii. Shearing can be directed to non-critical areas by adjusting the coverage: regions where shearing should be minimized should have a high coverage, while regions where shearing is required can be left unpatterned.

## CRediT authorship contribution statement

**Jan Philipp Janzen:** Methodology. **Hendrik Schäfer:** Methodology, Investigation, Data curation, Conceptualization. **Murat Çelik:** Writing – review & editing, Methodology, Investigation, Conceptualization. **Colin Robert:** Writing – review & editing, Methodology, Conceptualization. **Conchúr M.Ó Brádaigh:** Writing – review & editing, Methodology, Conceptualization. **David May:** Writing – review & editing, Methodology, Funding acquisition, Conceptualization. **Thomas Neumeyer:** Writing – review & editing, Resources, Methodology, Conceptualization.

## Funding

This work has been conducted within the framework of the project "NewPreg – Sustainable, economical and functionalised bio-solid resin prepreg technology for CO2 reduction through cooling-free storage, use of renewable resources and weight reduction through tailor-made draping properties" which is funded by the Federal Ministry of Economics and Climate Protection on the basis of a resolution of the German Bundestag (funding reference 20Q2227B).

## Declaration of competing interest

The authors declare that they have no known competing financial interests or personal relationships that could have appeared to influence the work reported in this paper.

## Data availability

Data linked to this study was published on Zenodo: 10.5281/zenodo.14646282

## References

[1] J. Sutter *et al.*, "Comparison of Autoclave and Out-of-Autoclave Composites," *Proceedings of SAMPE 2010*, vol. 2010, 2010. [Online]. Available: https://ntrs.nasa.gov/api/citations/20110016095/downloads/20110016095.pdf.

[2] M. Mehdikhani, L. Gorbatikh, I. Verpoest, S.V. Lomov, Voids in fiber-reinforced polymer composites: a review on their formation, characteristics, and effects on mechanical performance, J. Compos. Mater. 53 (12) (2019) 1579–1669, https://doi.org/10.1177/0021998318772152.

[3] T. Centea, L.K. Grunenfelder, S.R. Nutt, A review of out-of-autoclave prepregs – Material properties, process phenomena, and manufacturing considerations, Compos. A Appl. Sci. Manuf. 70 (2015) 132–154, https://doi.org/10.1016/j.compositesa.2014.09.029.

[4] M.H. Hassan, A mini review on manufacturing defects and performance assessments of complex shape prepreg-based composites, Int. J. Adv. Manuf. Technol. 115 (11–12) (2021) 3393–3408, https://doi.org/10.1007/s00170-021-07421-8.

[5] L.K. Grunenfelder, T. Centea, P. Hubert, S.R. Nutt, Effect of room-temperature out-time on tow impregnation in an out-of-autoclave prepreg, Compos. A Appl. Sci. Manuf. 45 (2013) 119–126, https://doi.org/10.1016/j.compositesa.2012.10.001.

[6] Y. Yu, H. Su, W. Gan, Effects of Storage Aging on the Properties of Epoxy Prepregs, Ind. Eng. Chem. Res. 48 (9) (2009) 4340–4345, https://doi.org/10.1021/ie8018005.

[7] J. Radanitsch. "Multi-layer carbon stacks for large wind turbine rotor blades." Accessed: Feb. 9, 2023. [Online]. Available: https://www.hexcel.com/innovation/Documents/Multi-layer%20carbon%20stacks%20for%20large%20wind%20turbine%20blades_CAMX%202014.pdf.

[8] P. Margueres, J. Lopez Torres, J.-N. Perie, K.S. Muhammad, F. Collombet, Combined Approach for the Characterization of Composites Manufactured by RFI and Industrial Application, J. Compos. Mater. 42 (2) (2008) 189–209, https://doi.org/10.1177/0021998307086200.

[9] P. Margueres, J.-N. Périé, J.G. Perez, F. Collombet, Y.-H. Grunevald, Characterization of a composite structure obtained by RFI using HexFIT® semi-products, Compos. Sci. Technol. 69 (1) (2009) 117–124, https://doi.org/10.1016/j.compscitech.2007.10.059.

[10] J. Summerscales, T.J. Searle, Low-pressure (vacuum infusion) techniques for moulding large composite structures, Proceed. Institut. Mechan. Eng., Part L: J. Mater.: Design Appl. 219 (1) (2005) 45–58, https://doi.org/10.1243/146442005X10238.

[11] Gurit. "Gurits SPRINT Data Sheet and Product Processing Guide." Accessed: Nov. 27, 2024. [Online]. Available: https://www.gurit.com/wp-content/uploads/2022/12/SPRINT-PROCESSING-Guide.pdf.

[12] Gurit. "Guide to Composites." Accessed: Nov. 13, 2023. [Online]. Available: https://www.gurit.com/wp-content/uploads/2022/12/guide-to-composites-1.pdf.

[13] W. Hu, S. Nutt, Effects of debulk temperature on air evacuation during vacuum bag-only prepreg processing, Adv. Manuf. Polym. Compos. Sci. 6 (1) (2020) 38–47, https://doi.org/10.1080/20550340.2020.1728476.

[14] S.G.K. Schechter, L.K. Grunenfelder, S.R. Nutt, Air evacuation and resin impregnation in semi-pregs: effects of feature dimensions, Adv. Manuf. Polym. Compos. Sci. 6 (2) (2020) 101–114, https://doi.org/10.1080/20550340.2020.1768348.

[15] J.P. Janzen, D. May, Solid epoxy prepregs with patterned resin distribution: Influence of pattern and process parameters on part quality in vacuum-bag-only processing, Polym. Compos. Art. no. pc.27696 (2023), https://doi.org/10.1002/pc.27696.

[16] S.G.K. Schechter, L.K. Grunenfelder, S.R. Nutt, Design and application of discontinuous resin distribution patterns for semi-pregs, Adv. Manuf. Polym. Compos. Sci. 6 (2) (2020) 72–85, https://doi.org/10.1080/20550340.2020.1736864.

[17] S.G.K. Schechter, T. Centea, S.R. Nutt, Polymer film dewetting for fabrication of out-of-autoclave prepreg with high through-thickness permeability, Compos. A Appl. Sci. Manuf. 114 (2018) 86–96, https://doi.org/10.1016/j.compositesa.2018.08.002.

[18] M. Préau and P. Hubert, "Processing of co-bonded scarf repairs: Void reduction strategies and influence on strength recovery," *Composites Part A: Applied Science and Manufacturing*, vol. 84, pp. 236–245, 2016. doi: 10.1016/j.compositesa.2016.01.016. [Online]. Available: https://www.sciencedirect.com/science/article/pii/S1359835X16000312.

[19] Solvay, "Technical Data Sheet VTM 260 Series Prepreg (ZPreg)," Accessed: Mar. 19, 2024. [Online]. Available: www.solvay.com.

[20] S.S. Tavares, Y. Roulin, V. Michaud, J.-A.-E. Månson, Hybrid processing of thick skins for honeycomb sandwich structures, Compos. Sci. Technol. 71 (2) (2011) 183–189, https://doi.org/10.1016/j.compscitech.2010.11.001.

[21] NEXX Technologies. "Datasheet - NTC-425 Cyanate Ester Prepreg." Accessed: Nov. 14, 2023. [Online]. Available: https://img1.wsimg.com/blobby/go/acb02ff0-7593-4e2f-b4bf-f93c5484f461/downloads/NTC425_DATASHEET%2009-06-2023.pdf?ver=1698778660083.

[22] M. Richardson. "NEXX Technologies unveils vertically integrated cyanate ester prepreg system." Accessed: Feb. 9, 2023. [Online]. Available: https://www.composites.media/nexx-technologies-unveils-vertically-integrated-cyanate-ester-prepreg-system.

[23] Y. Ming, S. Zhang, W. Han, B. Wang, Y. Duan, H. Xiao, Investigation on process parameters of 3D printed continuous carbon fiber-reinforced thermosetting epoxy composites, Addit. Manuf. 33 (2020) 101184, https://doi.org/10.1016/j.addma.2020.101184.

[24] H. Zhang, et al., 3D printing of continuous carbon fibre reinforced powder-based epoxy composites, Compos. Commun. 33 (2022) 101239, https://doi.org/10.1016/j.coco.2022.101239.

[25] M. Dickert, G. Ziegmann, Influence of Binder on the Mechanical Properties and the Permeability of a Non-Crimp Carbon Fabric Preform.

[26] O. Rimmel, D. Becker, P. Mitschang, Maximizing the out-of-plane-permeability of preforms manufactured by dry fiber placement, Adv. Manuf. Polym. Compos. Sci. 2 (3–4) (2016) 93–102, https://doi.org/10.1080/20550340.2016.1260900.

[27] O. Rimmel, D. May, P. Mitschang, Impact of stitching on permeability and mechanical properties of preforms manufactured by dry fiber placement, Polym. Compos. 40 (4) (2019) 1631–1642, https://doi.org/10.1002/pc.24911.

[28] T. Deringer, Integrative manufacturing of thermoset injection molding components with continuous fiber-reinforcement, Zeitschrift Kunststofftechnik 1 (2019) 169–187, https://doi.org/10.3139/O999.03022019.

[29] T. Deringer, D. Drummer, In situ curing and bonding of epoxy prepregs in epoxy thermoset injection molding, Int. J. Adv. Manuf. Technol. 117 (9–10) (2021) 2667–2677, https://doi.org/10.1007/s00170-021-07838-1.

[30] T. Deringer, C. Gröschel, D. Drummer, Influence of mold temperature and process time on the degree of cure of epoxy-based materials for thermoset injection molding and prepreg compression molding, J. Polym. Eng. 38 (1) (2018) 73–81, https://doi.org/10.1515/polyeng-2016-0409.

[31] T. Deringer, Methodik zur integrativen Kombination duroplastischer Formmassen und Prepregs im Spritzgießverfahren, Friedrich-Alexander-Universität Erlangen-Nürnberg (FAU), Doctoralthesis, 2022.

[32] M. Çelik, J.M. Maguire, T. Noble, C. Robert, C.M.Ó. Brádaigh, Numerical and experimental investigation of Joule heating in a carbon fibre powder epoxy towpregging line, Compos. A Appl. Sci. Manuf. 164 (2023) 107285, https://doi.org/10.1016/j.compositesa.2022.107285.

[33] M. Çelik, T. Noble, A. Haseeb, J. Maguire, C. Robert, C.M.Ó. Brádaigh, Contact resistance heating of unidirectional carbon fibre tows in a powder-epoxy towpregging line, Plast., Rubber Compos. 51 (8) (2022) 383–392, https://doi.org/10.1080/14658011.2022.2108982.

[34] M. Çelik, T. Noble, F. Jorge, R. Jian, C.M.Ó. Brádaigh, C. Robert, Influence of Line Processing Parameters on Properties of Carbon Fibre Epoxy Towpreg, J. Compos. Sci. 6 (3) (2022) 75, https://doi.org/10.3390/jcs6030075.

[35] A.G. Andreopoulos, P. Tarantili, Preparation and study of aramid/epoxy prepregs, J. Mater. Sci. 30 (8) (1995) 2159–2162, https://doi.org/10.1007/BF00353049.

[36] T. D. Bayha *et al., Processing, Properties and Applications of Composites using Powder-Coated Epoxy Towpreg Technology*, Advanced Composites Technology Conference. Accessed: Jan. 27, 2022. [Online]. Available: https://ntrs.nasa.gov/citations/19940010804.

[37] N. J. Johnston, Cano, R. J., Marchello, J. M., and D. A. Sandusky, *Powder-Coated Towpreg: Avenues to Near Net Shape Fabrication of High Performance Composites.* Accessed: Jan. 27, 2022. [Online]. Available: https://ntrs.nasa.gov/citations/19960023881.

[38] R. M. Baucom and J. M. Marchello, *LaRC Dry Powder Towpreg System.* Accessed: Jan. 27, 2022. [Online]. Available: https://ntrs.nasa.gov/citations/19920013396.

[39] J.M. Maguire, K. Nayak, C.M.Ó. Brádaigh, Characterisation of epoxy powders for processing thick-section composite structures, Mater. Des. 139 (2018) 112–121, https://doi.org/10.1016/j.matdes.2017.10.068.

[40] J.M. Maguire, P. Simacek, S.G. Advani, C.M.Ó. Brádaigh, Novel epoxy powder for manufacturing thick-section composite parts under vacuum-bag-only conditions. Part I: Through-thickness process modelling, Compos. A Appl. Sci. Manuf. 136 (2020) 105969, https://doi.org/10.1016/j.compositesa.2020.105969.

[41] J.M. Maguire, K. Nayak, C.M.Ó. Brádaigh, Novel epoxy powder for manufacturing thick-section composite parts under vacuum-bag-only conditions. Part II: Experimental validation and process investigations, Compos. A Appl. Sci. Manuf. 136 (2020) 105970, https://doi.org/10.1016/j.compositesa.2020.105970.

[42] J.M. Maguire, N.D. Sharp, R.B. Pipes, C.M.Ó. Brádaigh, Advanced process simulations for thick-section epoxy powder composite structures, Compos. A Appl. Sci. Manuf. 161 (2022) 107073, https://doi.org/10.1016/j.compositesa.2022.107073.

[43] C. M. Ó Brádaigh, A. Doyle, and D. Doyle, "Electrically-Heated Ceramic Composite Tooling for Out-of-Autoclave Manufacturing of Large Composite Structures," *Proceedings of SAMPE 2011*, 2011.

[44] M. Çelik, J.M. Maguire, H. Hasrin, T. Noble, C. Robert, C.M.Ó. Brádaigh, Impregnation behaviour during the production of powder epoxy towpregs, Compos. B Eng. 292 (2025) 112065, https://doi.org/10.1016/j.compositesb.2024.112065.

[45] J. Maguire, A. S. Roy, D. Doyle, M. Logan, and C. O Brádaigh, *Resin Characterisation for Numerical Modelling of Through-Thickness Resin Flow During OOA Processing of Thick-Section Wind or Tidal Turbine Blades: 20th International Conference on Composite Materials*.

[46] J.M. Maguire, J.-Y. Wang, C.M.Ó. Brádaigh, Hygroscopicity in Epoxy Powder Composites, Powders 3 (2) (2024) 168–189, https://doi.org/10.3390/powders3020011.

[47] J. P. Janzen, "Prozesskette zur Herstellung epoxidbasierter Feststoffharzprepregs und deren Verarbeitung zu Faser-Kunststoff-Verbunden," Dissertation, Leibniz-Institut für Verbundwerkstoffe, RPTU Kaiserslautern, 2025.

[48] M.A. Turk, B. Vermes, A.J. Thompson, J.-P.-H. Belnoue, S.R. Hallett, D.S. Ivanov, Mitigating forming defects by local modification of dry preforms, Compos. A Appl. Sci. Manuf. 128 (2020) 105643, https://doi.org/10.1016/j.compositesa.2019.105643.

[49] J. Pietschmann, *Industrielle Pulverbeschichtung: Grundlagen,Verfahren, Praxiseinsatz,* 4th ed. (JOT-Fachbuch Ser). Wiesbaden: Springer Fachmedien Wiesbaden GmbH, 2013. [Online]. Available: https://ebookcentral.proquest.com/lib/kxp/detail.action?docID=1636779.

[50] M. L. Berins, *SPI Plastics Engineering Handbook of the Society of the Plastics Industry, Inc*. Boston, MA: Springer US, 1991.

[51] S. Drücker, et al., Solid epoxy for functional 3D printing with isotropic mechanical properties by material extrusion, Addit. Manuf. 55 (2022) 102797, https://doi.org/10.1016/j.addma.2022.102797.

[52] L. Shen, et al., 3D Printable All-Polymer Epoxy Composites, ACS Appl. Polym. Mater. 3 (11) (2021) 5559–5567, https://doi.org/10.1021/acsapm.1c00889&ref=pdf.

[53] M.G. Wimmer, B.G. Compton, Semi-solid epoxy feedstocks with high glass transition temperature for material extrusion additive manufacturing, Addit. Manuf. 54 (2022) 102725, https://doi.org/10.1016/j.addma.2022.102725.

[54] Q. Jiang, H. Zhang, D. Rusakov, N. Yousefi, and A. Bismarck, "Additive Manufactured Carbon Nanotube/Epoxy Nanocomposites for Heavy-Duty Applications," *ACS Appl. Polym. Mater.*, early access. doi: 10.1021/acsapm.0c01011.

[55] P. Boisse, J. Colmars, N. Hamila, N. Naouar, Q. Steer, Bending and wrinkling of composite fiber preforms and prepregs. a review and new developments in the draping simulations, Compos. B Eng. 141 (2018) 234–249, https://doi.org/10.1016/j.compositesb.2017.12.061.

[56] R. Azzouz, S. Allaoui, R. Moulart, Composite preforming defects: a review and a classification, Int. J. Mater. Form. 14 (6) (2021) 1259–1278, https://doi.org/10.1007/s12289-021-01643-7.

[57] A. Rashidi, A.S. Milani, A multi-step biaxial bias extension test for wrinkling/de-wrinkling characterization of woven fabrics: Towards optimum forming design guidelines, Mater. Des. 146 (2018) 273–285, https://doi.org/10.1016/j.matdes.2018.02.075.

[58] *DIN 53362:2003-10, Prüfung von Kunststoff-Folien und von textilen Flächengebilden (außer Vliesstoffe), mit oder ohne Deckschicht aus Kunststoff_- Bestimmung der Biegesteifigkeit_- Verfahren nach Cantilever*, Berlin.

[59] T. Gereke, O. Döbrich, M. Hübner, and C. Cherif, "Experimental and computational composite textile reinforcement forming: A review," *Composites Part A: Applied Science and Manufacturing*, vol. 46, pp. 1–10, 2013. doi: 10.1016/j.compositesa.2012.10.004. [Online]. Available: https://www.sciencedirect.com/science/article/pii/S1359835X12003211.

[60] J. Xie, et al., Mechanics of textiles used as composite preforms: a review, Compos. Struct. 304 (2023) 116401, https://doi.org/10.1016/j.compstruct.2022.116401.

[61] S. Chen, A.J. Thompson, T.J. Dodwell, S.R. Hallett, J.-P.-H. Belnoue, Fast optimisation of the formability of dry fabric preforms: a Bayesian approach, Mater. Des. 230 (2023) 111986, https://doi.org/10.1016/j.matdes.2023.111986.

[62] P.H. Broberg, et al., One-click bending stiffness: Robust and reliable automatic calculation of moment–curvature relation in a cantilever bending test, Compos. B Eng. 260 (2023) 110763, https://doi.org/10.1016/j.compositesb.2023.110763.

[63] C. Krogh, K.D. White, A. Sabato, J.A. Sherwood, Picture-frame testing of woven prepreg fabric: an investigation of sample geometry and shear angle acquisition, Int. J. Mater. Form. 13 (3) (2020) 341–353, https://doi.org/10.1007/s12289-019-01499-y.

[64] *DIN EN ISO 20337:2020-01, Faserverstärkte Kunststoffe_- Schubversuch mittels Schubrahmen zur Ermittlung der Schubspannungs-/Schubverformungskurve und des Schubmoduls in der Lagenebene (ISO_20337:2018); Deutsche Fassung EN_ISO_20337:2019*, Berlin.

[65] I. Taha, Y. Abdin, S. Ebeid, Comparison of picture frame and Bias-Extension tests for the characterization of shear behaviour in natural fibre woven fabrics, Fibers Polym. 14 (2) (2013) 338–344, https://doi.org/10.1007/s12221-013-0338-6.

[66] J. Cao *et al.*, "Characterization of mechanical behavior of woven fabrics: Experimental methods and benchmark results," *Composites Part A: Applied Science and Manufacturing*, vol. 39, no. 6, pp. 1037–1053, 2008. doi: 10.1016/j.compositesa.2008.02.016. [Online]. Available: https://www.sciencedirect.com/science/article/pii/S1359835X08000572.

[67] E. Guzman-Maldonado, S. Bel, D. Bloom, P. Fideu, P. Boisse, Experimental and numerical analyses of the mechanical behavior during draping of non-orthogonal bi-axial non-crimp fabric composite reinforcements, Mater. Des. 218 (2022) 110682, https://doi.org/10.1016/j.matdes.2022.110682.

[68] P. Molnár, A. Ogale, R. Lahr, P. Mitschang, Influence of drapability by using stitching technology to reduce fabric deformation and shear during thermoforming, Compos. Sci. Technol. 67 (15–16) (2007) 3386–3393, https://doi.org/10.1016/j.compscitech.2007.03.022.

[69] H. Shen, P. Wang, X. Legrand, L. Liu, Characterisation and optimisation of wrinkling during the forming of tufted three-dimensional composite preforms, Compos. A Appl. Sci. Manuf. 127 (2019) 105651, https://doi.org/10.1016/j.compositesa.2019.105651.

[70] M. A. Abtew *et al.*, "Experimental investigation of effects of stitching orientation on forming behaviors of 2D P-aramid multilayer woven preform," in Palermo, Italy, 2018, p. 20001, doi: 10.1063/1.5034802.

[71] I. Gnaba, D. Soulat, X. Legrand, P. Wang, Investigation of the formability behaviour during stamping of tufted and un-tufted carbon preforms: towards localized reinforcement technologies, Int. J. Mater. Form. 14 (6) (2021) 1337–1354, https://doi.org/10.1007/s12289-020-01606-4.

[72] P. Matthäi, O. Döbrich, C. Cherif, Development of a Novel Technology for New Generation of Non-Crimp Fabrics – Manufacturing and simulation, AMR 936 (2014) 1821–1824, https://doi.org/10.4028/www.scientific.net/AMR.936.1821.

[73] M. Duhovic, P. Mitschang, D. Bhattacharyya, Modelling approach for the prediction of stitch influence during woven fabric draping, Compos. A Appl. Sci. Manuf. 42 (8) (2011) 968–978, https://doi.org/10.1016/j.compositesa.2011.03.025.

[74] M. A. Turk, H. Cao, A. J. Thompson, J. P.-H. Belnoue, S. R. Hallett, and D. S. Ivanov, "A New Approach to Measuring Local Properties of Preforms Enhanced for Formability," *Front. Mater.*, vol. 9, 2022, Art. no. 867591, doi: 10.3389/fmats.2022.867591.

[75] T.K. Nguyen, et al., Development of a novel direct powder screw extruder for 3D scaffold printing of PCL-based composites, Int. J. Adv. Manuf. Technol. 128 (7–8) (2023) 3161–3182, https://doi.org/10.1007/s00170-023-12076-8.

[76] M. Schöberl, K. Kasnakli, A. Nowak, Measuring strand orientation in carbon fiber reinforced plastics (CFRP) with polarization. *19th World Conference on Non-Destructive Testing*, 2016.

[77] D. Schommer, et al., Polarization imaging for surface fiber orientation measurements of carbon fiber sheet molding compounds, Compos. Commun. 37 (2023) 101456, https://doi.org/10.1016/j.coco.2022.101456.
[78] A. Albers *et al., Konstruktionselemente des Maschinenbaus 2: Grundlagen von Maschinenelementen für Antriebsaufgaben,* 8th ed. Berlin, Heidelberg: Springer Berlin Heidelberg, 2018. [Online]. Available: http://nbn-resolving.org/urn:nbn:de:bsz:31-epflicht-1531132.
[79] iwis GmbH, "Handbook for chain engineering: Design and construction/Examples of calculation," Accessed: Apr. 30, 2025. [Online]. Available: https://www.iwis.com/antriebssysteme/as-handbook/iwis-handbook-for-chain-engineering-design-and- construction.pdf.